Effective Local Deformation in Stretched Filled Rubber

ARTICLE *in* MACROMOLECULES · NOVEMBER 2003

Impact Factor: 5.8 · DOI: 10.1021/ma0303566

3 AUTHORS, INCLUDING:

J. Rault
Université Paris-Sud 11
76 PUBLICATIONS **1,239** CITATIONS

SEE PROFILE

Effective Local Deformation in Stretched Filled Rubber

S. Trabelsi, P.-A. Albouy, and J. Rault*

Laboratoire de Physique des Solides, UMR 8502, Université de Paris-Sud, Bâtiment 510, 91405 Orsay, France

Received June 26, 2003

ABSTRACT: The properties X (stress, crystallinity, melting temperature, crystallite sizes) of stretched filled and unfilled natural rubber (NR) are compared. The measurements have been done during deformation at equilibrium and at room temperature. From each physical property X in static and dynamic experiments one defines for the filled NR an amplification factor A_X and a differential amplification factor A^*_X. From stress and WAXS measurements two regimes are observed: For $\lambda < \lambda_A$, the material has not crystallized and the amplification factor A_X is independent of λ. A_X is on the order of 2 for the sample filled with 20% black carbon (volume concentration). It is shown that the Guth relation fits rather well our data and those of Lee and Donovan on similar filled NRs. For $\lambda > \lambda_A$, stress-induced crystallization occurs, $A_X \approx 1.5-3$ is weakly dependent on λ, and the differential amplification factor is constant. The values of A^*_X determined by the different measurements are of the same order of magnitude. These amplification factors characterize the state of extension of the amorphous chains during the process of stress-induced crystallization.

1. Introduction

Reinforcement of rubbers by barbon black (CB) and others types of filler particles (mean dimension 20−100 nm) is a process of great practical and technological importance.[1−5] In most cases CB increases the Young modulus,[6] fracture stress,[7] and wear and tear resistances.[8−10] The presence of small solid particles in rubber changes the stress field, increases the local strain of the chains, and leads to local heterogeneities.[11−14] It is well recognized that mechanical properties of these materials depend on the topology of the filler's surface and on the adsorption properties of the chains.[1,2] One of the key problems in understanding the mechanism of reinforcement is the following: what is the relation between local properties of the chains at the solid−rubber interface and far from the fillers; in other words, what is the relation between the macroscopic and local deformation, when the fillers are changed in nature (roughness, surface treatment, etc.) and concentration? In crystallizable rubbers such as natural rubber (NR), this question can be put in the following manner: what is the influence of the filler on the crystallization properties in the rubber matrix? One understands the importance of this question if one recalls that the excellent mechanical properties (tear resistance, crack propagation) of unfilled rubbers are due to the strain-induced crystallization (SIC).[15]

Guth and Gold[6] were the first authors to point out that the moduli E and E_f of unfilled and filled rubbers obey the law $E_f = A(c)E$. These authors noted that the coefficient $A(c)$ is a function of the filler concentration c. Mullins and co-workers[16−19] interpreted $A(c)$ as a strain amplification factor:

$$A = \epsilon/\epsilon_f = (\lambda - 1)/(\lambda_f - 1) \qquad (1)$$

(ϵ, ϵ_f) are respectively the mean local and macroscopic strains for filled rubbers and (λ, λ_f) are the corresponding draw ratios. Relationships between A and the filler content have been proposed on simple geometrical considerations by a few authors.[20,21] This factor was determined by comparing the stress−strain behaviors of unfilled, $\sigma(\lambda)$, and filled, $\sigma(\lambda_f)$, rubbers. To make these two behaviors coincide, one has simply to displace the filled stress−strain curve $\sigma(\lambda_f)$ to the higher draw ratios along the x axis. One postulates that, for the same value of the stress σ, the filled sample has a macroscopic draw ratio λ_f and local draw ratio λ. The effect of fillers, via the amplification factor, on the mechanical properties of various rubbers has been reviewed by Kraus[4] and Dannenberg et al.[5] Recently Reichert et al.[22] and Boyce et al.[23] gave rheological models based on the existence of a double network to describe the stress−strain behavior.

Recently Litvinov et al.[24−26] and Brierty et al.[27] used ^{1}H NMR to measure the dynamic and local deformation of the chains in filled PDMS networks. According to their studies, the physical adsorption of the elastomer chains to the surface of the filler causes a significant immobilization of the chains near the filler surface. In these noncrystalline PDMS rubbers, filled with 10% silica, Litvinov et al. observed two microregions with strongly different local chain mobilities: (1) a low mobile (semirigid) rubber layer which covers the filler surface and (2) a mobile (viscoelastic) elastomeric matrix outside this interface. The amplification factor determined by Litvinov and Spiess[25] shows that the local chain order at a given macroscopic elongation in a filled system is larger by a factor of 1.5−2 compared to that of the unfilled elastomer matrix. By small angle neutron scattering Westermann et al.[28] found an amplification factor on the order of 1.4−2 in microphase-separated triblock copolymer PI−PS−PI, the hard filler being the microphase of PS. Finally it has been emphasized that most carbon black rubbers are nonhomogeneous; carbon black aggregation and the microvoid[29] depend on the draw ratio (and the type of filler). Göritz et al.[14] by electron microscopy and by dilatometry in the presence of gauze of different nature arrived at the same conclusion. During deformation, zones of different morphologies are observed; strands connecting fillers appear parallel to the stretching direction. Crystallites are formed in these strands when the draw ratio reaches a

10.1021/ma0303566 CCC: $25.00
Published on Web 00/00/0000 PAGE EST: 6.5

Table 1

ingredient	NR	F-NR	ingredient	NR	F-NR
natural rubber (TSR 20)	100 g	100 g	antioxidant (6PPD)	1 g	1 g
carbon black (N375)	0 g	50 g	sulfur	1.2 g	1.2 g
stearic acid	2 g	2 g	accelerator (CBS)	1.2 g	1.2 g
zinc oxide	5 g	5 g			

critical value. In filled elastomers such as natural rubber, strain-induced crystallization occurs. The relation between the crystallization properties (crystallinity, crystallite morphology, ...) and the strain amplification factor has not been analyzed in detail to our knowledge.

The aim of this study is to compare the SIC properties of both types of rubbers, filled and nonfilled. From the variations of crystallinity, crystallite size, and melting temperature with draw ratio λ, one defines several strain amplification factors. One compares these various amplification factors with that deduced from the stress−strain curve.

2. Experimental Section

2.1. Materials. The materials (provided by Michelin) have been obtained by sulfur vulcanization of NR; their formulations are given by Table 1. Samples called here NR and F-NR have the same concentration of ingredients (stearic acid, zinc oxide, antioxidant, sulfur, and accelerator). Filled natural rubber (F-NR) contains 50 g of carbon black (N375) per 100 g (PHR) of polyisoprene. The concentration of the fillers in this case is 33% in weight (20% in volume). The cross-linking density ν_s of the unfilled natural rubber deduced from modulus and swelling measurements is $(5.7-6) \times 10^{-5}$ mol/cm^3. The number of monomers between cross-links is $N_C = \rho/M_0\nu_s = 238$; $M_0 = 68$ is the molecular weight of the monomer and $\rho = 0.92$ g/cm^3 the density of NR.

2.2. Instrument and Procedure. For the study of crystallization at a fixed draw ratio and at low temperature ($T_C = -25$ °C), a homemade oven with X-ray Kapton windows is used. The samples are thermalized between −30 °C and +100 °C. This oven is mounted onto a conventional ($\theta-2\theta$) goniometer (conventional generator, xenon-filled and proportional counter) or the front of a parallel beam optics (rotating anode generator, detection by CCD camera).

To measure simultaneously the crystallinity, stress, orientation, and size of crystallites during the cycle of stretching ($d\lambda/dt = 0.033$ min^{-1}) at room temperature, we used a drawing machine coupled with the above-mentioned CCD camera and mounted at station D 43 of the synchrotron LURE. In this case only the 002 reflection is recorded, the drawing machine being tilted to obtain this reflection.[32]

2.3. Data Correction and Analysis. **2.3.1. Crystallinity Measurements.** In static deformation, the crystallinity is deduced from the comparison between the intensity of the amorphous halo centered at 13.5 nm^{-1} in crystallized and melt states, in other words, at −25 °C and above the melting temperature of the sample, T_m. This method has already been explained in more detail by Dumbleton and Bowles[30] and used by others authors[10,31] for determining the crystallinity profile around a crack tip.

Using the relation established in static deformation between the crystallinity χ and the corresponding normalized intensity[31] I_{002}, we determined the crystallinity during cyclic deformation at room temperature. Normalization was done by the absorption measurement of the samples as explained in refs 31 and 32.

2.3.2. Crystallite Sizes and Orientation. From the line broadening (2θ) and the arc length of corrected reflection profiles, one measures, respectively, the size and the crystallite orientation. The crystallite sizes in the direction normal to the (hkl) planes are deduced from the Scherrer formula: $\langle l_{hkl}\rangle = K\lambda/(\beta_{1/2}\cos\theta)$, where $\beta_{1/2}$ is the angular half-width of corrected reflection profiles. This correction consists of subtracting the instrumental contribution which is given by the line profile of the quartz powder.

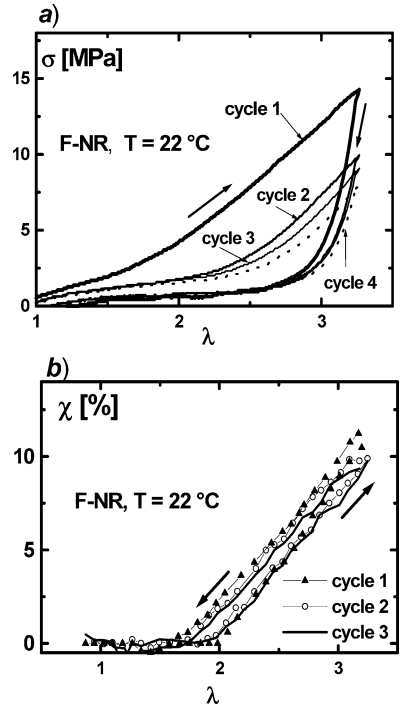

Figure 1. (a) Stress−strain curves of filled (F-NR) natural rubbers measured during mechanical cycles at $T = 22$ °C, strain rate 0.03 min^{-1}. After the first cycle the material shows a softening effect (Mullins effect). (b) Crystallinity measured at $T = 22$ °C during successive mechanical cycles as a function of the draw ratio.

3. Results and Discussion

3.1. Dynamics Experiments. 3.1.1. Stress Softening and SIC. To understand the effect of the stress softening on SIC during the cycle of stretching in filled rubbers, one has to measure simultaneously the tensile stress and the crystallinity during the four successive cycles for F-NR at $T = 22$ °C as a function of the strain (Figure 1). The strain rate is constant, 1 mm/min. It is well-known that after the first mechanical cycle a drop of the stress is observed; this is the so-called Mullins effect or stress softening. The fourth and fifth cycles are superposed. During different cycles, the crystallinity does not show any conspicuous difference. Also one has to verify that the orientation and crystallite sizes do not change from one cycle to another. One concludes that the Mullins effect does not play any role during stress-induced crystallization (stretching) and during melting (recovery). One recalls here that this Mullins effect appears also in noncrystallizable filled elastomers.

3.1.2. Measurements during Stable Cyclic Deformation. In Figure 2a are compared the stress−strain curves of filled (F-NR) and unfilled (NR) natural rubber samples drawn at 1 mm/min. The samples have been submitted first to four deformation cycles to obtain a stable cycle. The maximum draw ratios λ_{max} (arbitrarily chosen) are, respectively, 6 and 3 for these two types of materials.

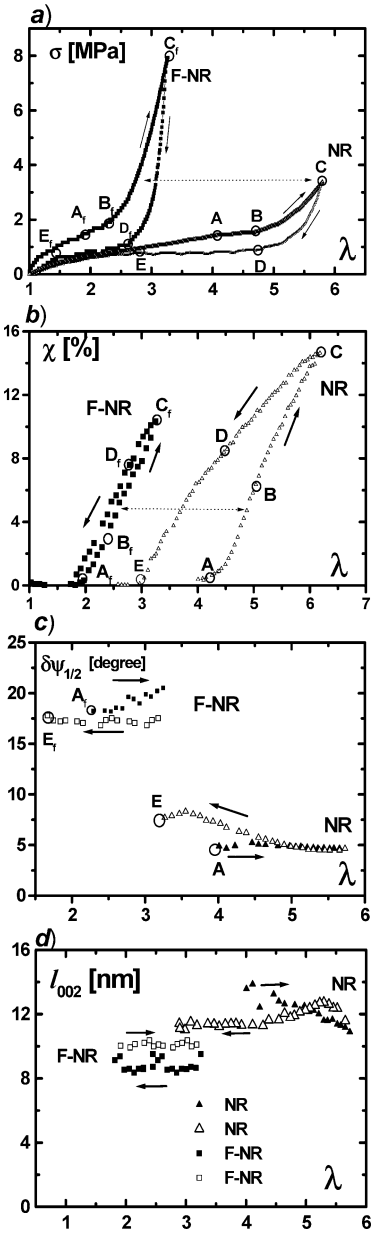

Figure 2. (a) Stress−strain curves of unfilled (NR) and filled (F-NR) natural rubbers (the measurements are done after the fourth mechanical cycle at 1 mm/min). Crystallization appears at draw ratios λ_{Af} (F−NR) and λ_A (NR). During recovery a plateau is observed between λ_D and λ_E for NR and between λ_{Df} and λ_{Ef} for F-NR. (b) Crystallinity measured during the mechanical cycle at room temperature. During traction the curves are parallel and can be superposed by a simple translation. (c, d) The crystallite size l_{002} and orientation $\delta\Psi_{1/2}$ remain constant for F-NR and NR during mechanical cycle.

As shown by various authors[1,18] the $\sigma(\lambda)$ curves (stretching and recovery) of filled sample can be superimposed with the unfilled curve by a simple orthogonal transformation along the λ axis. In the following by analogy with eq 1 for any physical property X (stress, crystallinity, melting temperature, crystallite sizes), the amplification factor A_X is definded by

$$A_X = \epsilon/\epsilon_f = (\lambda - 1)/(\lambda_f - 1) \qquad (2)$$

ϵ and ϵ_f are the strains of the unfilled and filled samples corresponding to the same value of property X. λ_f and λ are, respectively, the macroscopic and local draw ratios for filled natural rubber determined when $X(\lambda) = X(\lambda_f)$. The properties $X(\lambda)$ and $X(\lambda_f)$ concern, respectively, the unfilled and filled natural rubbers.

From the stress−strain curves (stretching) of Figure 2a, one notes that the amplification factor A_σ due to the presence of fillers is on the order of 3. When the maximum draw ratios λ_{max} of NR and F-NR samples are the same, one can verify that recovery curves $\sigma(\lambda)$ can be superposed with the same amplification factor.

In Figure 2b is reported the crystallinity χ measured during the cyclic deformation. The exposure time is 3 min; during this time one can consider that the sample has a fixed length. The important points to note are the following.

(a) Crystallization appears at $\lambda_A = 4$ for NR and $\lambda_{Af} = 2$ for F-NR somewhat before the beginning of the hardening, occurring at λ_B. In NR it has been shown that between these two draw ratios with the stress levels off, the plateau domain $\lambda_B - \lambda_A$ decreases with the cross-link density.[32] Due to the presence of the filler, this plateau, which is given in F-NR by $\lambda_{Bf} - \lambda_{Af}$, becomes much shorter than the NR one. This effect could be due to the covered filler particles by the semirigid interface, which can be considered as multifunctional physical cross-links as suggested by Litvinov et al.[26]

(b) During hardening ($\lambda > \lambda_B, \lambda_{Bf}$), due to the induced crystallites, which play the role of additional cross-links or fillers (for details cf. ref 32), the crystallinity of NR and F-NR varies linearly with deformation and with the same slope $d\chi/d\lambda$. The crystallinity curve $\chi(\lambda)$ during stretching (but not during recovery) of F-NR can be superimposed with that of the unfilled sample. The application of eq 2 leads to an amplification factor A_χ which varies from 3 to 2.25 when λ_f increases from 2 to 3.25; A_χ is on the order of A_σ.

(c) During recovery, one cannot define an amplification factor for the crystallinity; this suggests that in filled and unfilled NR the melting processes present some differences. One notes that the $\chi(\lambda)$ curve of F-NR presents a weak hysteresis compared to that of NR.

For both types of materials, the orientation and crystallite size l_{002} at $T = 22$ °C given in Figure 2c,d do not show any conspicuous variation with λ during the mechanical cycle. The same results are obtained for the three cross-linked samples studied,[32] which enables us to conclude that crystallization and melting proceed by formation or disappearance of the crystallite with constant morphology. F-NR and NR present however an important difference; the F-NR size l_{002} is about 9 nm, whereas the NR size is $l_{002} = 12$ nm. Also the crystallite orientations in these two materials are somewhat different; in F-NR the azimuthal angle $\delta\Psi_{1/2} \approx 20°$ is about twice the NR value, $\delta\Psi_{1/2} \approx 8°$. The lower orientation observed in filled rubber (for the same crystallinity, and therefore for different λ values) could be attributed to the elastomer−filler interface, which reveals a strong hindered chain mobility compared to the bulk.[27] Moreover, the filler surface could also affect the orientation of the crystallites due to a possible nucleating effect of the immobilized rubber−filler interface, and some chain ordering at the surface originated by the adsorption interactions.[25,26]

3.2. Static Experiments. 3.2.1. Crystallinity. In this experiment, F-NR and NR samples have also been submitted to several cycles of deformation until the stability of the mechanical cycle, the same conditions as for the dynamic experiment. The samples are drawn

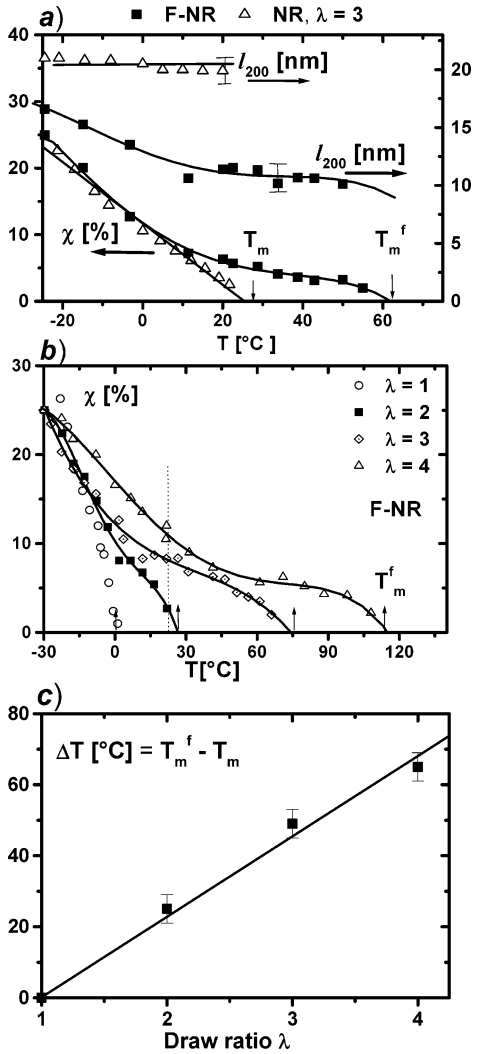

Figure 3. (a) Comparaison between NR and F-NR samples drawn at $\lambda = 3$ and then quenched to −25 °C. During heating the crystallinity χ and the crystallite sizes l_{200} are measured. (b) Crystallinity versus temperature of the F-NR samples drawn at different draw ratios, $1 \le \lambda \le 4$. (c) Difference ΔT between the melting temperatures of the F-NR and NR samples as a function of the draw ratio.

at 90 °C and then quenched to −25 °C. The samples are then heated by steps of 5 °C. At each temperature the WAXS is recorded; the mean time between two successive measurements at two temperatures is 10 min. In Figure 3a are compared the variations of the crystallinity of NR and F-NR samples with temperature; the samples have been drawn at $\lambda = 3$.

(a) At low temperature, $-25\ °C < T < T_0 = T_m - 15$ °C, the curves $\chi(T)$ of both types of samples coincide. In this domain, the extrapolated T_m value of the F-NR sample corresponds to the melting temperature of the unfilled sample, $T_m = 26$ °C, having the same draw ratio $\lambda = 3$.

(b) At higher temperature, $T > T_0 = 10$ °C, the crystallinity of F-NR remains constant. The plateau would correspond to highly extended regions, located near the fillers. Finally the crystallinity drops rapidly; the melting temperature $T_m{}^f$ of the filled sample is found by extrapolating $\chi(T)$ to zero.

In Figure 3b is given the crystallinity for F-NR versus T for different draw ratios $1 < \lambda < 4$. We observed that all curves converge to the same value, $\chi_{max} = 25\%$, at low temperature. At high temperature, the crystallinity

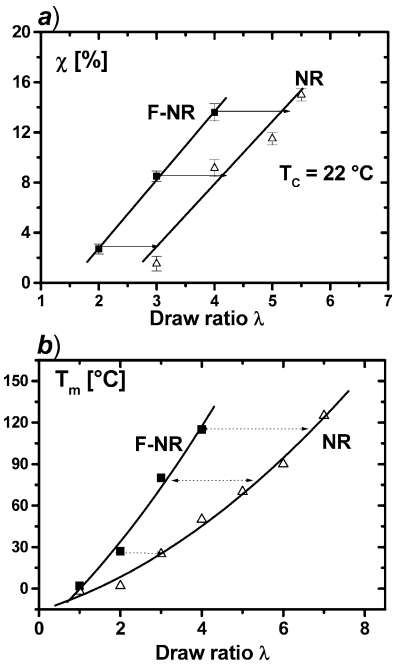

Figure 4. Crystallinity at room temperature (a) and melting temperature (b) of F-NR and NR samples versus the draw ratio. Coincidence of the curves can be obtained by the transformation $\lambda = A_\chi \lambda_f$ and $\lambda = A_T \lambda_f$, where A_χ and A_T are the amplification factors.

$\chi(T)$ presents a plateau independent of the draw ratio. Unfilled and filled rubber NR present different behaviors at high temperature (above T_0). At low temperature, $-25\ °C < T < T_0$, all curves of F-NR and NR coincide.

It has been shown in previous work on the same sample NR (see Figure 3 in ref 31) that the crystallinity varies linearly with T and the slope $d\chi/dT$ decreases linearly when λ varies from 1 to 6. This effect has been reported also by various authors.[9,31−34] By extrapolating the $\chi(T)$ curves (for $1 < \lambda < 6$) to zero at high temperatures, one determines the melting temperature T_m of the last crystallites in pure NR.

The presence of these two regimes in F-NR would be due to the presence of heterogeneous deformations as has been observed by Goritz et al.[14] on similar rubbers. The plateau value of the crystallinity, $\chi_p \approx 5-8\%$ ($\chi_{max} = 25\%$ in Figure 3a,b), suggests that this domain of high melting temperature ($T > T_0$) represents about 20% of the total crystal volume. These authors noted that crystallization appears first near the fillers and concluded that the local draw ratio near these fillers was higher than in the bulk. These two regions would have two different local draw ratios; the crystallites in these domains therefore have different melting temperatures $T_m{}^f$ and T_m. The difference $\Delta T = T_m{}^f - T_m$ between the melting temperatures of the filled and unfilled rubbers, respectively, given by the extent of the plateau and observed in Figure 3a,b, increases linearly with λ (Figure 3c).

In Figure 4a are compared the crystallinities of both types of samples at 22 °C as a function of the draw ratio. The crystallinity of filled and unfilled rubbers varies linearly with the draw ratio; the $\chi(\lambda)$ curve of the filled rubber can be superposed with the unfilled one by a simple translation along the λ axis. Application of eq 2 gives an amplification factor A_χ which varies from 2 to 1.3 when λ_f increases from 2 to 4; these values are somewhat smaller than those obtained (2.2−3) in dynamic experiments (Figure 2b).

3.2.2. Melting Temperatures. As shown by Figure 3a,b the melting proceeds progressively from −25 °C to T_m in the first region and rather abruptly in the second one near T_m^f. Here we report a new property: the states of the chain extension in the two regions are correlated; the melting temperatures verify the relation (Figure 3c):

$$\Delta T = T_m^{\ f} - T_m = B(\lambda - 1)\ (°C) \qquad (2)$$

The constant $B = 23$ °C in our case ($c = 33\%$ in weight). It would be interesting to measure this constant B for different filler concentrations c. One guesses here that this coefficient would decrease with c.

Figure 3c and eq 2 indicate clearly that the material cannot be visualized as a simple juxtaposition of independent domains of different extensions; the local draw ratios in these two domains are not independent.

In Figure 4b the melting temperatures $T_m(\lambda)$ and $T_m^f(\lambda)$ of both types of samples are compared. These temperatures are deduced from Figure 3 in ref 31 and Figure 3b here. One remarks again that the $T_m(\lambda)$ and $T_m^f(\lambda)$ curves can be superimposed. The amplification factor is $A_T = 2-1.8$ in the studied domain, $2 < \lambda_f < 4$.

3.2.3. Crystallite Sizes. In Figure 3a the variations of the crystallite size l_{200} measured along the transverse direction to the draw axis for filled and unfilled samples versus temperature are compared. The materials have been drawn at $\lambda = 3$. In unfilled NR this dimension (and the others,[32] l_{120}, l_{002}) decreases very slowly with T. In the filled sample the behaviors of l_{200} and χ are similar; the crystallite size l_{200} and the crystallinity χ first decrease linearly with T and then level off between $T_0 = 10$ °C and a temperature T, a few degrees (3−5 °C) below the melting temperature $T_m^f(\lambda_f = 3)$ of the filled sample. The remaining small crystals in the elastomer matrix do not melt despite the increase of the sample's temperature by ΔT on the order of 40 °C. This observed behavior of F-NR could be possibly explained by the mobility of the chain units hindered at the interface of the fillers. The immobilization effect of the chain segments absorbed on the filler would prevent the melting of small crystals near the filler surface.

In Figure 5a the value of the plateau is $l_{200} = 10$ nm for F-NR; one remarks that this value corresponds to a draw ratio $\lambda = 6$ in NR. In other words $\lambda = 6$ is the local draw ratio in F-NR, drawn at $\lambda_f = 3$. One concludes from these results that filled materials are heterogeneous and contain an overstrained region; this domain would represent 20% of the total crystal volume if we compare the crystallinity at the plateau, $\chi_p \approx 5\%$, with the maximum crystallinity obtained at low temperature, $\chi_{max} = 25\%$ (see Figure 3a,b).

Parts a and b of Figure 5 give the dimensions l_{200} and l_{002} of the crystallites along the (100) and (001) directions as a function of the draw ratio, measured at −25 °C; at this temperature the samples have the maximum of crystallinity, χ_{max}. At a fixed draw ratio λ, the crystallite size in F-NR measured along the stretching direction $l_C = l_{002}$ is higher than the NR one (see Figure 5b). The melting temperature T_f measurements given by Figure 4b confirm that the increase in T_f in F-NR is due to the increase of the crystallite size l_{002} (stem length).

The other dimension l_{120} does not vary conspicuously with λ. Here again one remarks that the curves $l_{200}(\lambda)$ and $l_{002}(\lambda)$ of both types of materials can be superimposed by displacements as shown by arrows in Figure 5a,b. Applying eq 2, one finds that the amplification factors A_l are on the order of 2.5−1.5 (l_{200}) and 1.7−1.4 (l_{002}). In ref 32 it is shown that crystallite sizes follow the affine law; the dimension along the draw ratio increases with λ, and the transverse dimension decreases. The volume of the crystallites being constant is proportional to $V_C = l_{200}l_{002}l_{120}$. The volumes V_C measured at −25 °C of filled and unfilled rubbers (Figure 5c) are equal and independent of the draw ratio. For unfilled NR it has been found that the mean crystallite volume V_C is constant when the temperature increases up to the melting temperature; this is a characteristic of the affine deformation, which should be verified for filled NR.

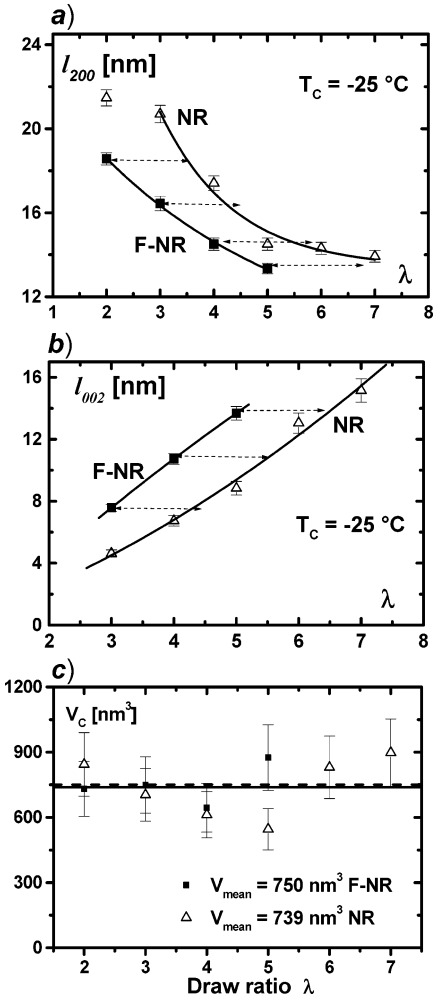

Figure 5. Comparison between F-NR and NR samples at −25 °C, crystallite sizes (a, b) and crystallite volume V_C as a function of the draw ratio.

4. Conclusion

The mechanical and morphology properties of filled and unfilled natural rubbers during SIC have been compared. By varying the temperature, one finds that the filled rubber exhibits two different behaviors: at low temperature the crystallinity curves χ(T) of filled and unfilled rubbers coincide but the size curves $l_{200}(T)$ do not. At low temperature one can verify that the sizes of the crystallites follow the affine deformation for both types of materials. At higher temperature (for $T > T_0$), the observation of a plateau in the $l_{200}(T)$ and $\chi(T)$ curves (in the same temperature range) is accounted for by the presence of distinct regions where the local

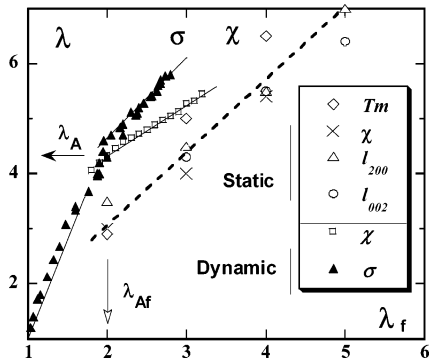

Figure 6. Draw ratio λ of the unfilled NR as a function of the corresponding draw ratio λ_f of the filled F-NR sample. At each point (λ, λ_f) the two different samples have the same property X (X being T_m, χ, l_{200}, l_{002}, or σ). The properties X are measured in static and/or dynamic experiments. Arrows indicate the draw ratios at the onset of crystallization during stretching.

Table 2

	amplification factor values	draw ratio domain
A_σ (dynamic deformation)	$A_\sigma = 3$	for $1 < \lambda_f < 2$
	$2.5 < A_\sigma(\lambda_f) < 3$	for $2 < \lambda_f < 3$
A_χ (dynamic deformation)	$2.25 < A_\chi(\lambda_f) < 3$	$2 < \lambda_f < 3.25$
A_χ (static deformation)	$1.3 < A_\chi(\lambda_f) < 2$	$2 < \lambda_f < 4$
A_T (static deformation)	$1.8 < A_T(\lambda_f) < 2$	$2 < \lambda_f < 4$
A_l (static deformation)	l_{200}, $1.5 < A_l < 2.5$	$2 < \lambda_f < 5$
	l_{002}, $1.4 < A_l < 1.7$	

stresses (and strains) are different. In the bulk far from the fillers the local stress has the same value as in unfilled rubber. Near the fillers (aggregated or isolated) the stress is much higher.

In Figure 6 for any value of the property X (static and dynamic) we have plotted the draw ratio λ of the unfilled NR as a function of the draw ratio λ_f of the filled NR and then postulated that λ_f is the macroscopic deformation and λ the local one of the filled sample. In the figure the dashed line is the best linear fit with all the static data (χ, T_m, l_{002}, l_{200}). The amplification factors A_σ, A_χ, A_{T_m}, and $A_{l_{002}}$ deduced from stress−strain, crystallinity, melting temperature, and crystallite size measurements are on the order of 1.3−3 when λ_f varies from 2 to 5. This is summarized in Table 2.

The general relation between the local and the macroscopic draw ratios λ and λ_f in static and dynamic deformations can be put in the following form:

$$\lambda = (\lambda_A - A_X^*\lambda_{Af}) + A_X^*\lambda_f \qquad (3)$$

λ_A and λ_{Af} are the draw ratios for the onset of crystallization in NR and F-NR samples. We call A_X^* the differential amplification factor. All the curves $\lambda(\lambda_f)$ have constant slope, $A_X^* = d\lambda/d\lambda_f$, when crystallization has appeared ($\lambda > \lambda_{Af}$).

The curve $\lambda(\lambda_f)$ deduced from the stress−strain curve (triangles in the figure) exhibits two different regimes, $A^*_\sigma = A_\sigma = 3$ for $\lambda_f < \lambda_{Af}$ and $A_\sigma^* = 1 \pm 0.2$ for $\lambda_f > \lambda_{Af}$. The change of regime appears very abruptly at the onset of SIC ($\lambda_{Af} = 2$). It is important to remark that the differential amplification factors A_X^* in the domain $\lambda > \lambda_{Af}$ are on the order of 1 ± 0.2 whatever the property analyzed. Then eq 3 gives the local draw ratio $\lambda = (\lambda_A - \lambda_{Af}) + \lambda_f$, where the constant $\lambda_A - \lambda_{Af}$ is on the order of 1−2 depending on the property X.

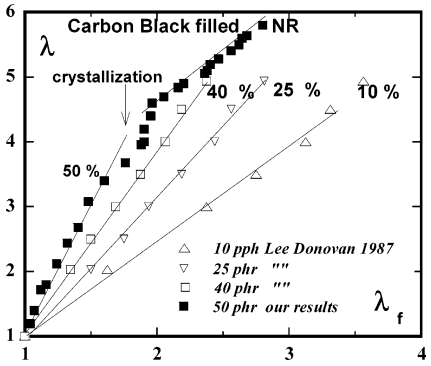

Figure 7. Comparison of the $\lambda(\lambda_f)$ curves of various filled F-NR samples deduced from stress−strain curves at room temperature. Open symbols: results of Lee and Donovan (10, 25, and 40 phr). Filled squares: mechanical results of Figure 6 (50 phr).

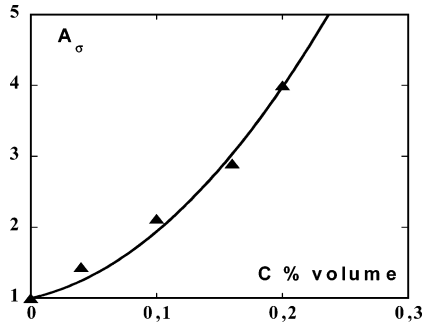

Figure 8. Amplification factor A_σ of filled samples F-NR of Figure 7 as a function of the volume concentration of the filler. The heavy line represents the best fit with the Guth relation (eq 4).

In Figure 7 are given the results of Lee and Donovan[10] (deduced from the stress−strain curves of their Figure 12). Their samples were filled with 10, 25, and 40 phr of HAF carbon black; this corresponds to volume concentrations of 4%, 10%, and 16%. It is not clear why the two different regimes are not observed on their stress−strain curves (no plateau AB as observed in Figure 2a) and on the $\lambda(\lambda_f)$ curves. In our opinion this would be due to the strain rate used for the stress−strain experiments. We have verified that when the strain rate increases the crystallinity decreases[35] (for the same value of the stress during stretching). Despite this difference, one can verify that the slope $d\lambda/d\lambda_f$ decreases with the concentration. In Figure 8 is reported the amplification factor $A_\sigma = \epsilon/\epsilon_f = d\lambda/d\lambda_f$ observed before the onset of crystallization ($A_\sigma = A_\sigma^*$) as a function of the volume concentration of carbon black. The heavy line in the figure is the best fit with the Guth and Gold relation:[6]

$$A_\sigma = (\lambda - 1)/(\lambda_f - 1) = (1 + 0.67\alpha c + 1.62\alpha^2 c^2), \quad \alpha = 5.8 \qquad (4)$$

c is the volume concentration of the filler, and the correlation factor is $R = 0.992$. The fit parameter $\alpha = 5.8$ corresponds rather well with the value $\alpha = 6.7$ found by Mullins and Tobin[16] on similar materials (see the review of Kraus[4]). Litvinov and Spiess[24] found a similar value for Aerosil-filled PDMS networks. It is worthwhile to note that the above relation can be replaced by the empirical linear relation $A_\sigma = 1 + 12c$, the correlation factor being on the same order. The accuracy of the measurements and the small number of data impede

any relevant discussion on the origin of the above relation. It would be interesting to know how the interaction between absorbed chains and the filler surface modify the two amplification factors A_X and A^*_X.

To summarize, from WAXS study of stress-induced crystallization in filled and unfilled natural rubbers one can deduce two different strain amplification factors, $A_X \approx 2$ and $A^*_X \approx 1$, in agreement with the stress−strain measurements. Other filled rubbers were studied to verify if these amplification factors are dependent on the nature of the elastomer.

Acknowledgment. We thank Dr. P. Johnson and Dr. J. M. Favrot from Michelin for stimulating discussions and remarks about this work.

References and Notes

(1) Kraus, G. *Reinforcement of Elastomers*; Interscience Publishers: New York, London, Sydney, 1965; p 64.
(2) Donnet, J. B.; Voet, A. *Physics, Chemistry and Elastomer Reinforcement*; Marcel Dekker: New York, Basel, 1976.
(3) Kraus, G.; Childers, C. W.; Rollmann, K. W. *J. Appl. Polym. Sci.* **1966**, *10*, 229.
(4) Kraus, G. *Adv. Polym. Sci.* **1971**, *8*, 155.
(5) Dannenberg, M.; Brennan, J. J. *Rubber Chem. Technol.* **1965**, *39*, 597.
(6) (a) Guth, E.; Gold, O. *Phys. Rev.* **1938**, *53*, 322. (b) Guth, E.; Gold, O. *J. Appl. Phys.* **1945**, *16*, 20.
(7) Kinloch, A. J.; Young R. J. *Fracture Behaviour of Polymers*; Elsevier: London, 1983; p 370.
(8) Greensmith, H. W. *J. Polym. Sci.* **1956**, *21*, 175.
(9) Gent, A. N. *Rubber Chem. Technol.* **1996**, *69*, 834.
(10) Lee, D. J.; Donovan, J. A. *Rubber Chem. Technol.* **1987**, *V60*, 15, 910.
(11) Bueche, F. *Physical Properties of Polymers*; Wiley-Interscience: New York, 1962.
(12) Hess, W. M. *Rubber Chem. Technol.* **1962**, *35*, 228.
(13) (a) Mass, S.; Gronski, W. *Kautsch. Gummi Kunstst.* **1994**, *47*, 328. (b) Mass, S.; Gronski, W. J. *Rubber Chem. Technol.* **1995**, *68*, 652.
(14) Goritz, D. *Angew. Makromol. Chem.* **1992**, *202/203*, 309.
(15) (a) Gent, A. N. *Engineering with Rubber*; Hanser Publishers: Oxford University Press: Oxford, 1992. (b) Gent, A. N. *Science and Technology of Rubber*; Academic Press: New York.
(16) Mullins, L.; Tobin, N. R. *J. Appl. Polym. Sci.* **1965**, *9*, 2993.
(17) Mullins, L. *Rubber Chem. Technol.* **1969**, *42*, 339.
(18) Harwood, J. A. C.; Mullins, L.; Payne, A. R. *J. Appl. Polym. Sci.* **1965**, *9*, 3011.
(19) Harwood, J. A. C.; Payne, A. R. *J. Appl. Polym. Sci.* **1966**, *10*, 315, 1203.
(20) Bueche, F. *J. Appl. Polym. Sci.* **1961**, *5*, 271.
(21) Bueche, A. M. *J. Appl. Phys.* **1952**, *23*, 154.
(22) Reichert, W. F.; Goritz, D.; Duschl, E. J. *Polymer* **1993**, *34*, 1216.
(23) Bergstrom, J. S.; Boyce, M. C. *Mech. Mater.* **2000**, *32*, 627.
(24) Litvinov, V. M.; Spiess, H. W. *Makromol. Chem.* **1991**, *192*, 3005.
(25) Litvinov, V. M.; Spiess, H. W. *Makromol. Chem.* **1992**, *193*, 1181.
(26) Litvinov, V. M.; Steeman. *Macromolecules* **1999**, *32*, 25, 8476.
(27) McBrierty, V. J.; Kenny, J. C. *Kautsch. Gummi Kunstst.* **1994**, *47*, 342.
(28) Westermann, S.; Kreitschmann, M.; Pyckhout-hintzen, W.; Richter, D.; Straube, E. *Physica B* **1997**, 306.
(29) Reichert, W. F.; Hopfenmuller, M. K.; Goritz, D. *J. Mater. Sci.* **1987**, *22*, 3470.
(30) Dumbleton, J. H.; Bowles, B. B. *J. Polym. Sci., Part A* **1966**, *4*, 951.
(31) Trabelsi, S.; Albouy, P. A.; Rault, J. *Macromolecules* **2002**, *35*, 10054.
(32) Trabelsi, S.; Albouy, P. A.; Rault, J. *Macromolecules* **2003**, *36*, 7624.
(33) Taylor, G. R.; Darin, S. R. *J. Appl. Phys.* **1955**, *26*, 1075.
(34) Alexander, L. E.; Ohlberg, S.; Taylor, G. R. *J. Appl. Phys.* **1955**, *26*, 1068.
(35) Trabelsi, S. Thesis, Orsay, 2002.

MA0303566